J Mater Sci (2008) 43:6912–6919
DOI 10.1007/s10853-008-2996-0

Preparation of NiAl–TiC nanocomposite by mechanical alloying

M. Zakeri · M. R. Rahimipour · A. Khanmohammadian

Received: 14 May 2008 / Accepted: 5 September 2008 / Published online: 27 September 2008
© Springer Science+Business Media, LLC 2008

Abstract NiAl–TiC nanocomposite was successfully synthesized via a ball-milled mixture of Ni, Al, Ti, and graphite powders. The structural and morphological evolutions of the powders were studied by X-ray diffraction (XRD) and scanning electron microscopy (SEM), respectively. Results show that NiAl–TiC composite was obtained after 6 h of milling. The mean grain sizes of 6 and 10 nm were attained for NiAl and TiC at the end of milling, respectively. An annealing of 3 h milled sample at 600 °C led to the formation of Ni (Al, Ti, C) solid solution. NiAl–TiC nanocomposite that was formed in the 12 h milled sample is stable during an annealing at 600 °C. The mean grain size of NiAl at the 12 h milled powder increased during annealing at 600 °C. Maximum micro hardness value of 870 kg/mm^2 (8.7 GPa) was acquired from the 12 h milled powder. SEM images and particle size measurement showed that very fine spheroid particles (1 μm) were procured at the end of milling.

Introduction

NiAl, as promising intermetallics, can be used as a high-temperature material due to its high melting point, low density, specific modulus, excellent thermal conductivity, and good oxidation resistance. However, cast polycrystalline NiAl suffers from low ambient temperature ductility and poor creep resistance at service temperature [1–3]. In an effort to overcome these shortcomings, developing a nanocrystalline NiAl strengthened by a second phase may be a promising way, since the ductility can be improved by the refined microstructure [4] and the creep resistance can be enhanced by the reinforced particulates [5].

The formation of alloys via solid-state reaction that occurs during ball milling of elemental powders, called mechanical alloying (MA), is a promising way of producing such composites [6–8]. During MA both matrix and reinforcement are formed through in situ process, which will promote good bonding between matrix and reinforcement. Moreover, a homogeneous distribution of fine reinforcing particles can be obtained by the MA process [9, 10].

The mechanical properties of these alloys can be improved by reinforcing them with particles such as TiC. A further improvement of mechanical properties can be achieved by decreasing the grain size to the nanometer scale. Zhou et al. [11] synthesized a NiAl–TiC nanocomposite by the MA of Ni, Al, Ti, and C powders. They suggested two separate explosive reactions that simultaneously occur and complete gradually. They did not investigate the properties of the as-milled powders. In another research, several Ni–Al–Ti–C compositions from different areas of the Ni–Al phase diagram containing various amounts of Ti and C were prepared by MA [12]. They concluded that the solid-state reaction in the MA process of Ni–Al–Ti–C mixtures proceeded in various ways and depended on the ratio of Ni and Al in the mixture. They obtained a nanocomposite with a grain size <5 nm. In this study, as in the previous case, mechanical properties were not studied.

M. Zakeri (✉) · A. Khanmohammadian
Ceramic Department, Islamic Azad University
(Saveh Branch), P.O. Box 39187/366, Saveh, Iran
e-mail: M_zakeri@IAU-Saveh.ac.ir

M. R. Rahimipour
Ceramic Department, Materials and Energy Research Center,
Tehran, Iran

The aim of this work is to obtain NiAl–TiC nanocomposite directly during low periods of milling. Micro-hardness, structural, and morphological evolutions were studied and more relevant discussions are performed on the X-ray diffraction (XRD) profile analyses.

Experimental

MA was performed in a planetary ball mill at nominal room temperature with a vial rotation speed (cup speed) of 600 rpm. Pure Merck Ni, Al, Ti, and graphite (99.9%) powders were mixed to give the desired NiAl (75)–TiC (25) wt% composition. The ball-to-powder weight ratio (BPR) was 12:1. Five balls with 20 mm, four ball with 15 mm, and five balls with 10 mm of diameter were used in the MA experiments. Energy of the ball mill can be increased by using a distribution of balls with different sizes. Ball size distribution increases the frequency of the ball–ball and ball–wall impacts and leads to the higher energy of the ball mill [13]. The mixture of the powders and the steel balls was charged into a steel vial (150 mL) in Ar atmosphere. Samples for analysis were removed by interrupting the ball mill at various intervals.

XRD profiles were recorded on a Philips diffractometer (30 kV and 25 mA) with Cu $K\alpha_1$ radiation ($\lambda = 1.5404$ A°). All XRD experiments were done with a step size of 0.02° and a time per step of 1 s. The recorded XRD patterns were used for the calculation of crystallite size and strain. Prior to calculations from the XRD peaks, the background was automatically removed and the $K\alpha_2$ radiation (Eq. 1) was stripped from the scans using the computer software X-pert High Score developed by PANalytical B. V. company (Netherlands).

$$K\alpha_2/K\alpha_1 = 0.51. \tag{1}$$

X-Pert High Score uses the Pseudo-Voigt profile function (Eq. 2), which is the weighted mean between a Lorentz and a Gaussian function:

$$G_{ik} = \gamma \frac{C_0^{1/2}}{H_k \pi} \left[1 + C_0 X_{ik}^2\right]^{-1} + (1-\gamma) \frac{C_1^{1/2}}{H_k \pi^{1/2}} \exp\left[-C_1 X_{ik}^2\right], \tag{2}$$

where $C_0 = 4$, $C_1 = 4 \times \ln 2$, H_k is the full-width at half-maximum (FWHM) of the kth Bragg reflection, $X_{ik} = (2\theta_i - 2\theta_k)/H_k$. γ is a variable mixing parameter, describing the amount of Gaussian profile versus the amount of Lorentzian profile and thus describing the overall profile shape.

Structural observations of the milled powders were carried out with a Philips CM200 FEG transmission electron microscope (TEM) operating at 200 kV. The morphology and the particle size of the mechanically alloyed powders were examined by a Philips scanning electron microscope (SEM) operating at 25 kV. Heat treatment of as-milled powders was performed in a tube furnace in Ar atmosphere (2.2 L/min). The heating rate was 10 °C/min and the holding time at the maximum temperature was 2 h.

For micro-hardness investigations, the milled and annealed powders were mounted and carefully ground and polished. Vickers micro-hardness measurements were performed on the mounted and polished powders under a load of 25 g and a dwell time of 10 s.

Results and discussion

Figure 1 shows the XRD patterns of the as-received powder mixture and after different milling times. The as-received powder mixture consisted of Ni, Al, Ti, and graphite that had been mixed on the stoichiometry of the following reactions (Ratio of NiAl: TiC, 75:25 wt.% was selected):

$$\begin{aligned} &Ni + Al \rightarrow NiAl \\ &Ti + C \rightarrow TiC. \end{aligned} \tag{3}$$

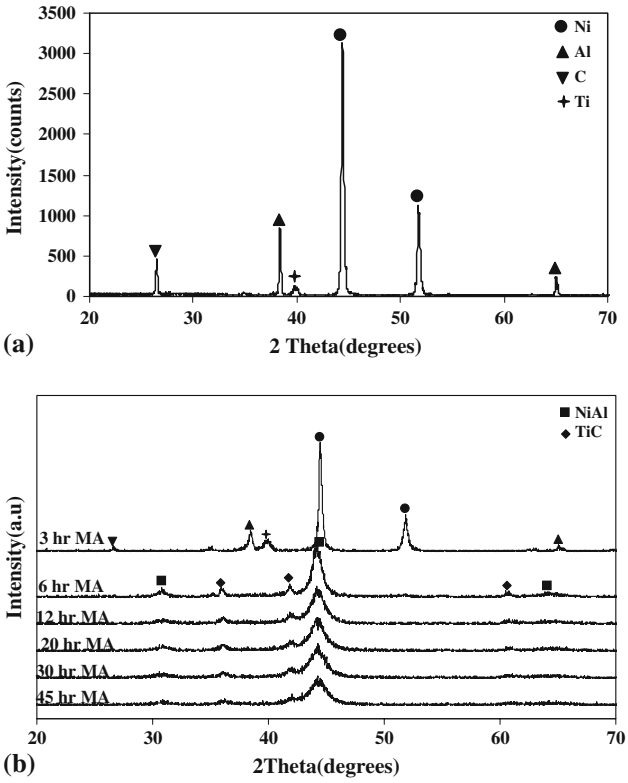

Fig. 1 XRD patterns of powder mixtures **a** as-received and **b** after different milling times

In the early stage of milling (3 h), only the XRD peaks of Ni were broadened and a strong decrease in Ti, Al, and C XRD peak intensities took place. Lack of any shift in the Ni peak positions leads to the conclusion that no reciprocal solid solution has occurred. It seems that the process of intimate mixing in the early stages of milling was responsible, to a large extent, for the decrease in the intensity of Ti, Al, and C reflections. The large difference between the mass absorption coefficient of the Ni and the other mentioned elements leads to absorption of the intensities of Ti, Al, and C reflections by Ni [10]. Grain size reduction and intimate mixing of the ball-milled elements lead to a resonance in this phenomenon. As seen in Fig. 1 after 6 h of MA the XRD peaks of the raw material virtually disappeared. It is due to the reaction between Ni, Al, Ti, and C to form NiAl and TiC phases based on the above reactions. Due to short period of reaction (6 h), it may be occurred in the explosive mode. For determination of the exact reaction mode, the temperature of the vial must be recorded during milling, which is not performed in this study. With increasing the milling time to 45 h, no further reaction took place and only the XRD peaks broadened.

The apparent size of NiAl and TiC crystallites was calculated from the broadening of XRD peaks. Each XRD line profile obtained in a diffractometer is broadened due to instrumental and physical (crystallite size and lattice strains) factors. Therefore, the first indispensible step for the calculation of crystallite size and lattice strain from the recorded XRD scan is the determination of the pure diffraction line profile for a given reflection [14]. This pure line profile is extracted by removing (de-convoluting) the instrumental broadening factor from the experimental line profile. Only then the pure line profile can be used for calculating the crystallite size and lattice strain.

Simple equations or graphs based on line profiles of assumed analytical forms can be used for the instrumental broadening correction. In the present work, the instrumental broadening was removed based on the following equation [14]:

$$B^2 = b^2 + \beta^2, \tag{4}$$

where B and b are the integral breadth (IB) (in radians) of the same Bragg peak from the XRD scans of the experimental and reference powder, respectively. The reference powder was the nickel powder annealed at 800 °C for 6 h. Both B and b were calculated by the computer software X-Pert High Score as the FWHM after automatic background removal and $K\alpha_2$ stripping. Also IB was used for its better accuracy [14]. IB is the width of a rectangle having the same area and peak height as the actual line profile. Due to the overlapping and the large broadening of the synthesized phases, calculations were performed on the [110] and [111] reflections of the NiAl and TiC, respectively.

In order to calculate the mean crystalline size, the well-known Scherrer method was applied [15]. In this method, it is assumed that the broadening is due to the very fine grains and the effect of the lattice strain is not taken into account; therefore the results have some inaccuracy. A reverse condition is assumed to obtain the lattice micro strain.

$$d = \frac{\lambda}{\beta \cos\theta}$$

Scherrer equation for mean grain size calculation, (5)

$$\eta = \frac{\beta}{4\tan\theta}$$ Micro strain calculation, (6)

where λ is the X-ray wavelength (nm), θ the peak position (radians), β the pure line profile breadth (radians), d the average volume of mean grain size (nm), and η is the lattice micro-strain. Figure 2 shows the mean grain size and microstrain evolution of NiAl and TiC versus the ball milling time, simultaneously. Both phases exhibited the similar behavior. The longer milling times led to the lower mean grain size and the higher microstrain. There was no considerable difference between the FWHM and IB results and it can be neglected. Changing rate (slope of curves) of mean grain size and microstrain at the shorter milling times is very significant. In contrast, at longer milling times, the evolution rate becomes trivial. These mean that there is equilibrium at the end of milling. This is confirmed on the basis of fitted equations. It means that there is no considerable change in the calculated values at higher milling times. At the end of milling, the mean grain size of NiAl and TiC reached the approximately constant values of 5 and 10 nm, respectively. On the other hand, the lattice microstrain of NiAl and TiC got to 1.8 and 1.2%, respectively.

To obtain more information, the exact peak position (2θ) and the atomic plane space (d space) were measured. Peak position (2θ) was found based on the fitted function. The atomic plane space (d space) was calculated by Bragg equation ($n\lambda = 2d\sin\theta$) [14]. Figure 3 shows the results of calculation for NiAl and TiC simultaneously. The [110] and [111] reflections were used for NiAl and TiC calculations, respectively. In both phases, increasing the milling time resulted in a shift in the XRD peak positions to higher angles, indicating a decrease in d spacing. This phenomenon can be explained based on the solid solution theory. In this theory, the shift of reflections to higher angles means that a solute element with smaller size has been dissolved in the solvent lattice [15]. Solid solution of NiAl such as Ni(Al, Ti) is likely. Similarly, solid solution of TiC as

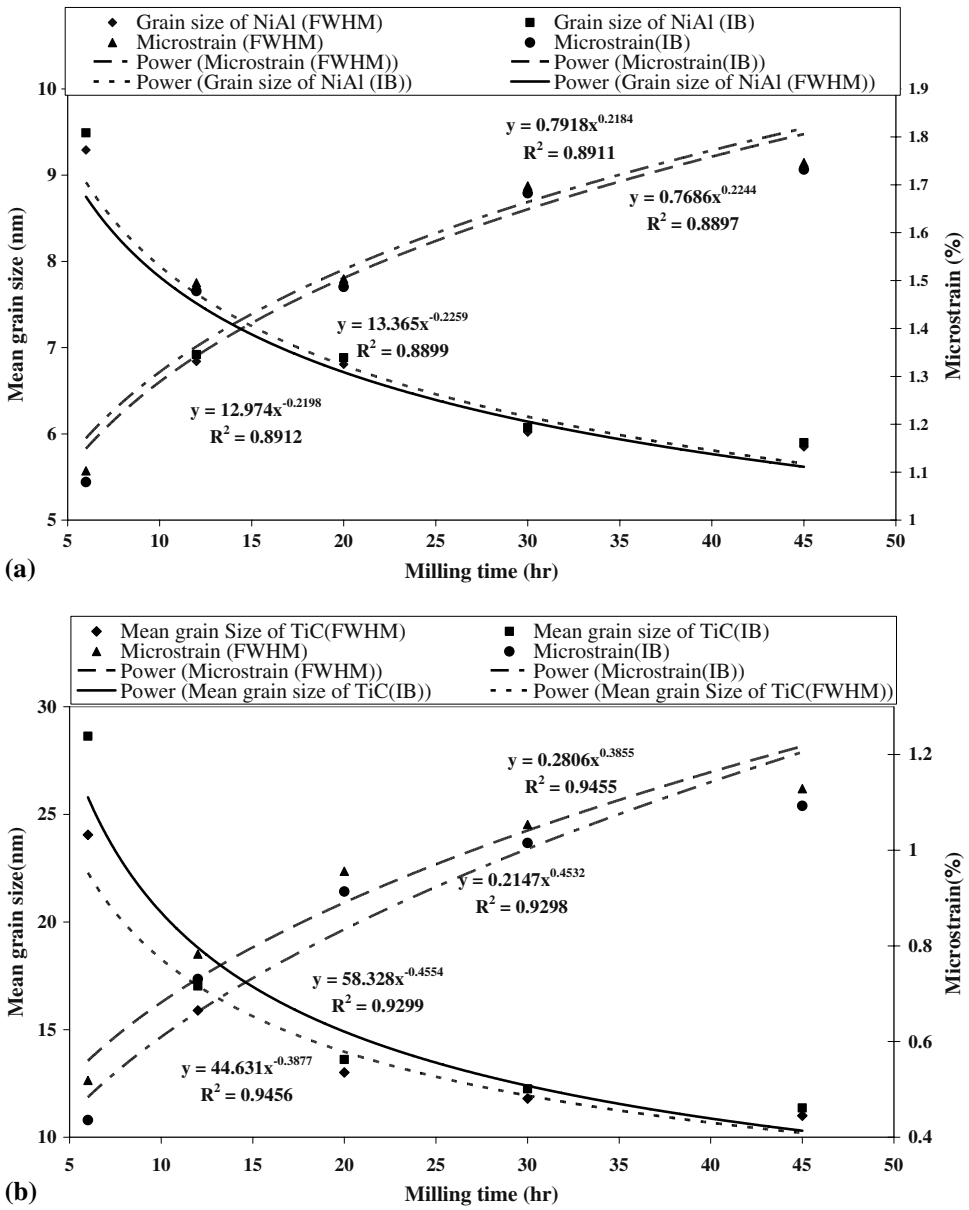

Fig. 2 Mean grain size and lattice microstrain calculation results for **a** NiAl and **b** TiC

(Ti,Ni)C is possible. The in situ result of falling *d* space is increasing in the corresponding peak position. As the mean grain size and lattice microstrain was discussed, there is equilibrium in the calculated parameters at the end of milling, which is confirmed on account of the fitted equations. As it can be seen, the slope of the curves decreases at longer milling times and reach to 0, approximately.

Structural evolution of the as-milled powder (3 h) was studied after an annealing at 600 and 1000 °C for 2 h. Figure 4a shows the XRD patterns of this sample after an annealing. The as-milled powder includes Ni, Al, Ti, and C (Fig. 1). As seen, none of Ti, Al, and C exists in the XRD pattern. And also the main XRD peak of Ni shifts to the lower angle. It means that the three disappeared element XRD peaks (Ti, Al, and C) were solved in the Ni lattice. Theses results indicate that in the annealing of 3 h milled sample at 600 °C, solid solution formation is thermodynamically and kinetically favor to intermetallic (NiAl) formation. Annealing at 1000 °C had no interesting results. This sample included Ni and C remained from starting materials as major phases. Also TiC and Ni_3Al were formed as minor phases.

Thermal stability of NiAl–TiC nanocomposite structure was investigated by annealing the 12 h milled powder at 600 and 1000 °C for 2 h. Figure 4b shows the XRD patterns of this sample after annealing. The as-milled powder includes NiAl and TiC phases (Fig. 1). No new phase was formed after annealing at 600 °C. It means that this is the

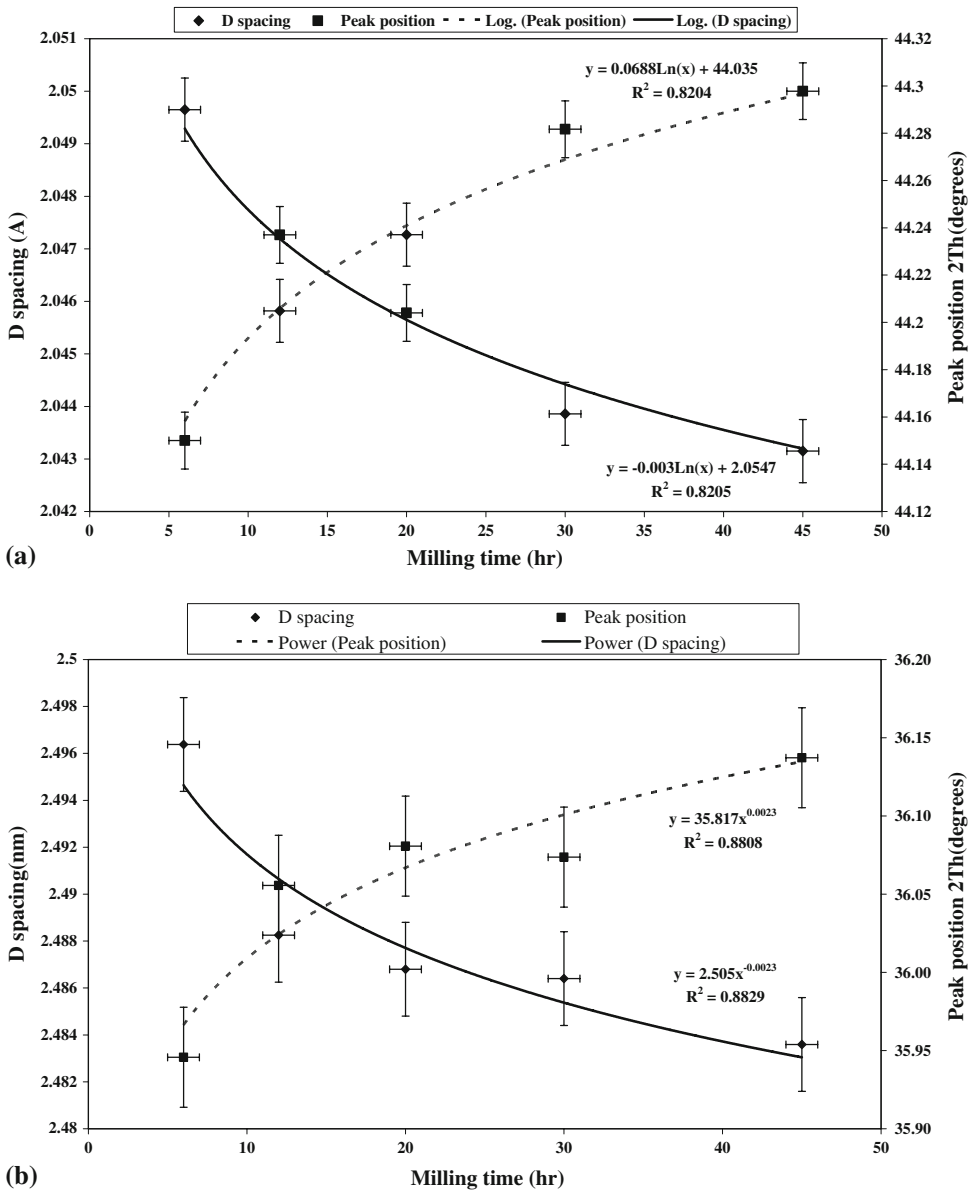

Fig. 3 Peak position and *d* spacing calculation results of **a** NiAl and **b** TiC

best condition for synthesizing of NiAl–TiC nanocomposite or it is stable until 600 °C. On the other hand, more than NiAl and TiC, three new phases of $Ni_{1.1}Al_{0.9}$, Ni_3 (Al, Ti), and Ti_8C_5 were synthesized after annealing at 1000 °C.

The width of XRD peaks decreased and their intensity increased after an annealing due to stress releasing as well as grain growth. Table 1 shows results of the mean grain size and microstrain before and after an annealing at 600 °C. As it is illustrated, the mean grain size increased and the microstrain was released after annealing at 600 °C. There is no significant difference between IB and FWHM results.

The average Vickers microhardness value (ten indents on each sample) of the milled and annealed samples is shown in Fig. 5. The standard deviation of the measured values is quite small (2%). The average microhardness of the powder particles increased substantially as the milling time rose from 3 to 12 h. This value is approximately fixed in the range from 12 to 20 h of milling. With further milling, this value decreases to 540 kg/mm^2 (5.4 GPa), due to the recovery process during milling [15]. An annealing performed on the 3 h milled powders led to complete hardening due to the formation of Ni_3Al and TiC (Fig. 4a). On the other hand, an annealing of 12 h milled powders resulted in complete softening due to the grain growth and strain releasing (Table 1).

Figure 6 shows the SEM micrographs of the milled powders for different times. The milled powders after 3 h (Fig. 6a) include very large particles and agglomerates. Particle and agglomerate sizes decrease with increasing the

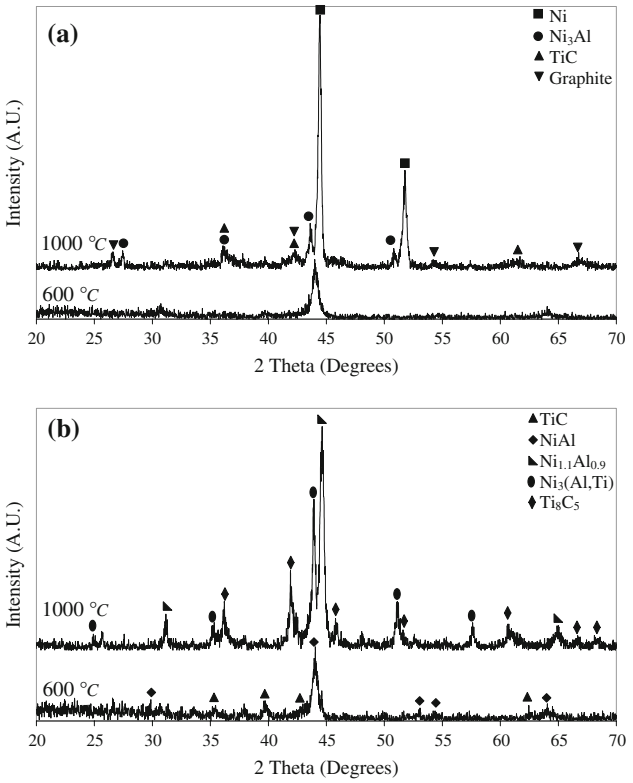

Fig. 4 XRD patterns of annealed powders after **a** 3 h and **b** 12 h of milling time

milling time (Fig. 6b–d). These agglomerates consist of very fine particles that are cold welded together (Fig. 6f) due to the very hard plastic deformation. As the milling time is increased, the powder particles become finer and more homogeneous in their structure. Figure 6e shows the fine microstructure of the 45 h milled sample at higher magnification. Average particle size of the milled powders was measured by using SEM images. Diameters of 300 particles were used for this measurement. Figure 7 shows the results of this measurement. As it is observed, the longer milling time led to a decrease in the mean particle size. It can be noted that the mean particle size got to the approximately fixed value of 1 μm at the end of milling. This is corroborated by the fitted equation. It means that the fitted equation have an asymptote at 1 μm.

The microstructure and indexed selected area diffraction pattern (SADP) of the 45 h milled sample observed in TEM are shown in Fig. 8. The rings in the SADP allow us to identify the NiAl and TiC phases. The first and second rings belong to TiC (200) and (220), respectively, and the third is attributed to NiAl (211). The rings indicate a very small size of crystallites (nanostructure) of both phases. Dark field image (Fig. 8a) and bright field image (Fig. 8b) show that the mean grain size of both phases is <10 nm. Thus, the mean crystallite size estimated using XRD method is approximately

Table 1 Mean grain size and microstrain calculation results of the 12 h milled sample

NiAl 12 h MA	Mean grain size (nm) (FWHM)	Mean grain size (nm) (IB)	Microstrain (%) (FWHM)	Microstrain (%) (IB)
Before annealing at 600 °C	6.8	6.9	1.5	1.5
After annealing at 600 °C	17.1	18.5	0.6	0.5

Fig. 5 Average Vickers microhardness at 25 g load of ball milled and annealed powders

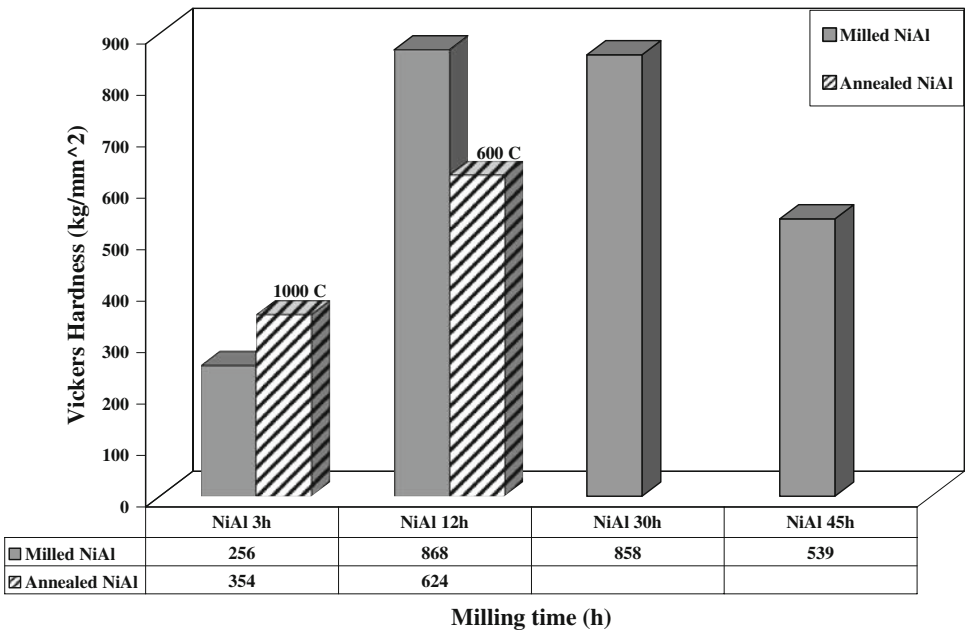

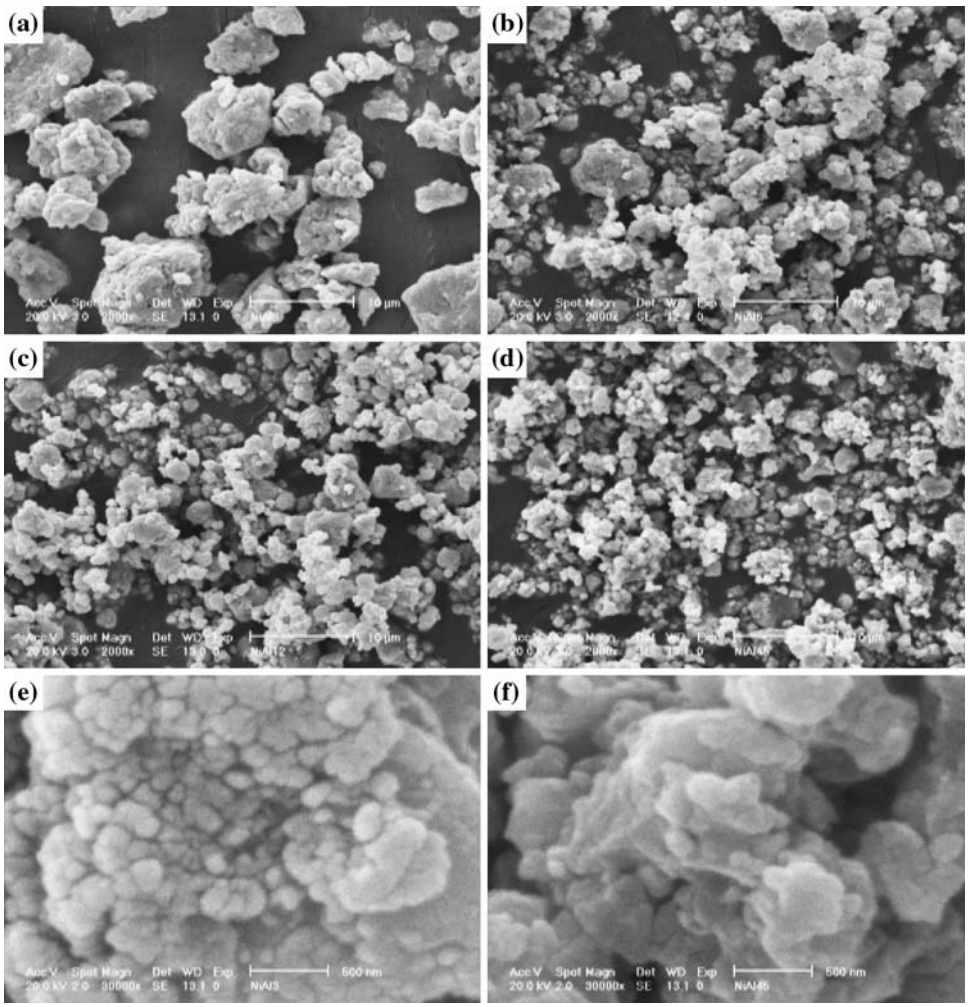

Fig. 6 SEM micrographs of the milled powders for **a** 3 h, **b** 6 h, **c** 12 h, **d** 45 h, **e** microstructure of the 45 h milled powder at higher magnification and **f** typical agglomerate at the end of milling

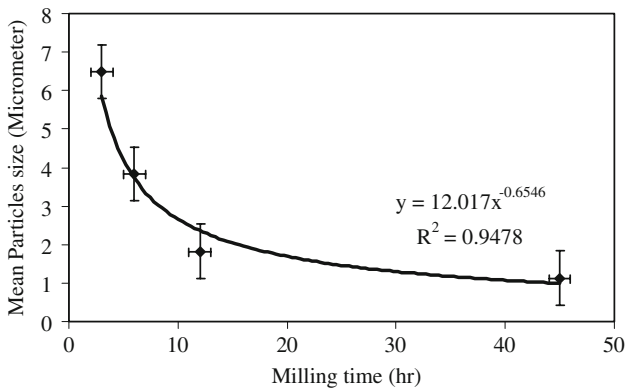

Fig. 7 Mean particle size of the milled powders measures by SEM images

consistent with TEM observations (refer to Fig. 2). Figure 8c shows energy dispersive analysis of Fig. 8a. As seen there are reflections of Ni, Al, Ti, and C in the XRD pattern that confirm the composition of NiAl–TiC composite.

Conclusion

NiAl–TiC nanocomposite was successfully synthesized by ball milling mixture of Ni, Al, Ti, and graphite powders. This composite was formed in the 6 h milled sample. At the end of milling, the mean grain sizes of NiAl and TiC were 6 and 10 nm, respectively. Additionally, maximum microstrain of 1.8 and 1.2% were procured for the 45 h milled NiAl and TiC, respectively. An annealing of 3 h milled sample at 600 °C led to the formation of Ni (Al, Ti, C) solid solution. NiAl–TiC nanocomposite that was formed in the 12 h milled sample is stable during an annealing at 600 °C. Undesired phases of Ni_3Al, $Ni_{1.1}Al_{0.9}$, $Ni_3(Al, Ti)$, and Ti_8C_5 were formed after an annealing of 3 and 12 h milled samples at 1000 °C. The mean grain size

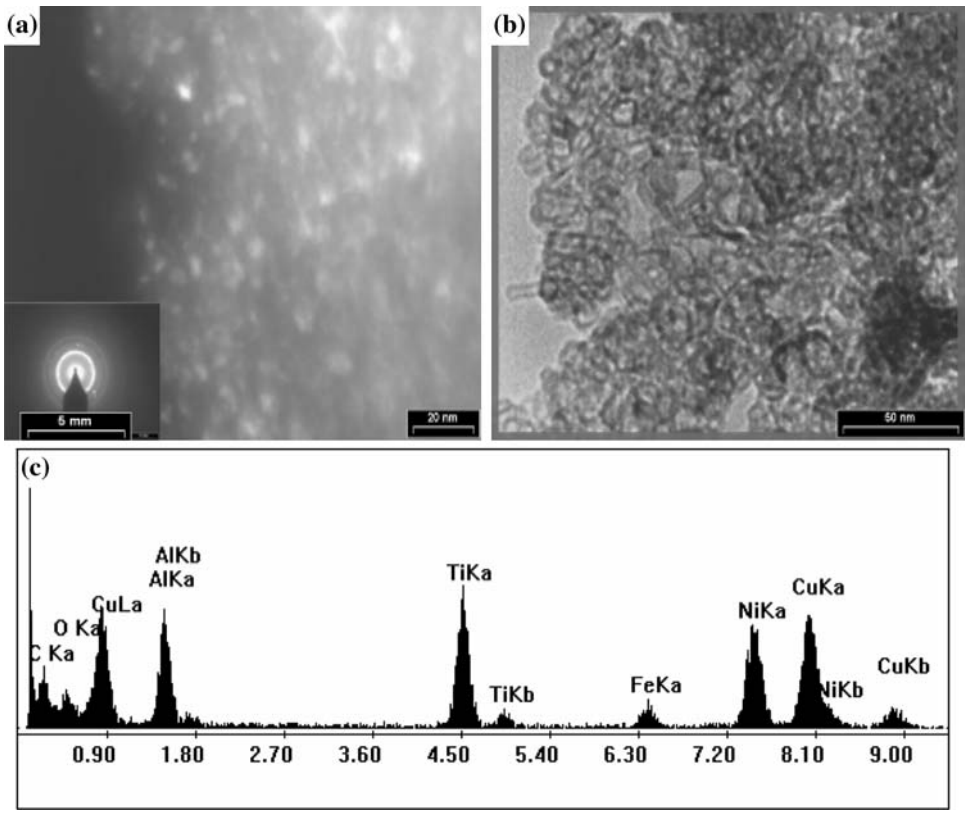

Fig. 8 TEM dark field image and SADP of the 45 h milled powder

and microstrain of the 12 h milled NiAl got to 18 nm and 0.5% after annealing at 600 °C, respectively. The maximum microhardness value of 870 kg/mm^2 (8.7 GPa) was obtained in the 12 h milled powder. An annealing of this sample led to a decrease in the microhardness to 620 kg/mm^2 (6.2 GPa). A very fine powder with the mean particle size of 1 μm was achieved at the end of milling.

References

1. Miracle DB (1993) Acta Metall Mater 41:649. doi:10.1016/0956-7151(93)90001-9
2. Dymek S, Dollar M, Hwang SJ, Nash P (1992) Mater Sci Eng A 152:160. doi:10.1016/0921-5093(92)90062-6
3. Khodaei M, Enayati MH, Karimzadeh F (2008) J Mater Sci 43:132. doi:10.1007/s10853-007-2123-7
4. Gleiter H (1989) Prog Mater Sci 33:223. doi:10.1016/0079-6425(89)90001-7
5. Wang L, Beck N, Arsenaut R (1994) J Mater Sci Eng A 177:83. doi:10.1016/0921-5093(94)90480-4
6. Zakeri M, Yazdani-Rad R, Enayati MH, Rahimipoor MR (2006) Mater Sci Eng A 430:185. doi:10.1016/j.msea.2006.05.112
7. Koch CC (2007) J Mater Sci 42:1403. doi:10.1007/s10853-006-0609-3
8. Reddy BSB, Das K, Das S (2007) J Mater Sci 42:9366. doi:10.1007/s10853-007-1827-z
9. Koch CC (1998) Mater Sci Eng A 244:39. doi:10.1016/S0921-5093(97)00824-1
10. El-Eskandarany MS (2001) Mechanical alloying for fabrication of advanced engineering materials. Noyes Publication, Norwich, NY
11. Zhou LZ, Guo JT, Fan G (1998) J Mater Sci Eng A 249:103. doi:10.1016/S0921-5093(98)00576-0
12. Krivoroutchko K, Kulik T, Matyja H, Portnoy VK, Fadeeva VI (2000) J Alloy Comp 308:230. doi:10.1016/S0925-8388(00)00802-1
13. Cullity BD (1977) Elements of X-ray diffraction, 2nd edn. Addison-Wesley Publishing, MA
14. Klug HP, Alexander L (1974) X-ray diffraction procedures for polycrystalline and amorphous materials, 2nd edn. Wiley, New York
15. Syrayanarayana C (2001) Prog Mater Sci 46:1. doi:10.1016/S0079-6425(99)00010-9